Journal of Cellular Biochemistry 100:617–628 (2007)

Nucleo-cytoplasmic Cycling of the Vitamin D Receptor in the Enterocyte-Like Cell Line, Caco-2

Anna Klopot,[1] Kenneth W. Hance,[1] Sara Peleg,[2] Julia Barsony,[3] and James C. Fleet[1]*

[1]Department of Foods and Nutrition and the Interdepartmental Nutrition Program, Purdue University, West Lafayette, Indiana 47907-2059
[2]Department of Endocrine Neoplasia and Hormonal Disorders, The University of Texas MD Anderson Cancer Center, Houston, Texas 77030
[3]Laboratory of cell Biochemistry and Biology, National Institute of Diabetes and Digestive and Kidney Diseases, National Institutes of Health, Bethesda, Maryland 20892

Abstract We examined the effects of 1,25 dihydroxyvitamin D_3 ($1,25(OH)_2D_3$) on the distribution and mobility of the vitamin D receptor (VDR) in the enterocyte-like Caco-2 cell. Confocal microscopy showed that a green fluorescent protein-vitamin D receptor (GFP-VDR) fusion protein is predominantly nuclear (58%) and it does not associate with the apical or basolateral membrane of proliferating or polarized, differentiated cells. In contrast to the previously studied cell types, neither endogenous VDR nor GFP-VDR levels accumulate in the nucleus following $1,25(OH)_2D_3$ treatment (100 nM, 30 min). However, in nuclear photobleaching experiments nuclear GFP-VDR import was significantly increased by $1,25(OH)_2D_3$ during both an early (0–5 min) and later (30–35 min) period (20% per 5 min). Compared to the natural ligand, nuclear import of GFP-VDR was 60% lower in cells treated with the $1,25(OH)_2D_3$ analog, 1-alpha-fluoro-16-ene-20-epi-23-ene-26,27-bishomo-25-hydroxyvitamin D_3 (Ro-26-9228, 5 min, 100 nM). Downstream events like ligand-induced association of VDR with chromatin at 1 h and the accumulation of CYP24 mRNA were significantly lower in Ro-26-9228 treated cells compared to $1,25(OH)_2D_3$ (60 and 95% lower, respectively). Collectively our data are consistent with a role for ligand-induced nuclear VDR import in receptor activation. In addition, ligand-dependent VDR nuclear import appears to be balanced by export, thus accounting for the lack of nuclear VDR accumulation even when VDR import is significantly elevated. J. Cell. Biochem. 100: 617–628, 2007.

Key words: intestine; nuclear trafficking; 1,25 dihydroxyvitamin D_3

Intestinal calcium absorption is a critical step in the maintenance of calcium homeostasis [Fleet, 2006]. It occurs by both paracellular and transcellular pathways [Bronner, 2003; Hoenderop et al., 2005]. The transcellular calcium absorption pathway is an active process that is regulated by the active form of vitamin D, 1,25 dihydroxyvitamin D_3 ($1,25(OH)_2D_3$). 1,25 $(OH)_2D_3$ increases efficiency of transcellular Calcium absorption by increasing the abundance of critical proteins: calbindin D_{9k} (CaBPD9k), the transient receptor vanelloid family member

Abbreviations used: CaBPD9k, calbindin D_{9k}; CRM-1, chromosomal region maintenance 1 protein; CYP24, 25-hydroxyvitamin D_3 24-hydroxylase; DMEM, Dulbecco's Modified Eagle's Medium; FBS, fetal bovine serum; GFP-VDR, chimera of green fluorescent protein with VDR; GRIP1, glucocorticoid receptor interacting protein; Ham's F12, Ham's nutrient mixture F12; ITS, insulin–transferrin–selenium; NLS, nuclear localization sequence; PCR, polymerase chain reaction; PI, propidium iodide; PR, phenol red; pRL-CMV, expression vector for Renilla luciferase; PMCA1b, plasma membrane calcium ATPase 1b; $1,25(OH)_2D_3$, 1,25 dihydroxyvitamin D_3; Ro-26-9228, 1-alpha-fluoro-16-ene-20-epi-23-ene-26,27-bishomo-25-hydroxyvitamin D_3; TFIIB, general transcription factor II B; TRPV6, transient receptor vanelloid family member 6; VDR, vitamin D receptor.

Anna Klopot and Kenneth W. Hance contributed equally to the work.

Grant sponsor: NIH; Grant number: DK54111; Grant sponsor: NIH; Grant number: DK50583.

Kenneth W. Hance's present address is Cancer Prevention Fellowship Program, Division of Cancer Prevention, National Cancer Institute, National Institutes of Health, Bethesda, MD 20892.

*Correspondence to: James C. Fleet, PhD, 700 West State St., Purdue University, West Lafayette, IN 47907-2059. E-mail: fleet@purdue.edu

Received 14 April 2006; Accepted 11 July 2006

DOI 10.1002/jcb.21087

6 (TRPV6), and the plasma membrane calcium ATPase 1b (PMCA1b) [Fleet et al., 2002; Song et al., 2003b; Fleet, 2006].

The actions of $1,25(OH)_2D_3$ are mediated by the vitamin D receptor (VDR), a transcription factor that belongs to nuclear hormone receptor superfamily [Haussler et al., 1998]. The deletion of VDR in the enterocyte results in a 70% reduction in intestinal calcium absorption efficiency that is coincident with a significant reduction in CaBPD9k, TRPV6, and PMCA1b gene expression [Van Cromphaut et al., 2001; Song et al., 2003a]. Previous research shows that binding of $1,25(OH)_2D_3$ to VDR in the cytoplasm of cells stimulates heterodimerization of VDR with RXR and the redistribution of the VDR-RXR-hormone complex to the nucleus [Barsony et al., 1990; Michigami et al., 1999; Racz and Barsony, 1999; Sunn et al., 2001]. The nuclear import of the VDR-RXR-hormone complex is active [Racz and Barsony, 1999; Miyauchi et al., 2005], enhanced by $1,25(OH)_2D_3$ treatment [Michigami et al., 1999; Racz and Barsony, 1999; Sunn et al., 2001], dependent upon the presence of intact nuclear localization sequences (NLSs) in both VDR and RXR [Prufer et al., 2000], and requires various importins [Miyauchi et al., 2005; Yasmin et al., 2005]. Most of the studies examining the mechanism of VDR nuclear import have been conducted in COS-7 kidney cells (characterized by low expression of endogenous VDR) and some characteristics of VDR import have been confirmed in cells from bone, skin, or kidney. In contrast the impact of $1,25(OH)_2D_3$ treatment on VDR distribution has not been examined in absorptive enterocytes, a primary target cell of $1,25(OH)_2D_3$ action.

In this article we have examined the nucleocytoplasmic trafficking of VDR receptor in proliferating and differentiated Caco-2 cells. Caco-2 cells are an intestinal cell line that spontaneously differentiates and recapitulates many of the features of the absorptive epithelial cell of the small intestine, including vitamin D regulated intestinal calcium absorption [Giuliano and Wood, 1991; Fleet et al., 2002]. We find that VDR nuclear import occurs under basal conditions and that import is accelerated by $1,25(OH)_2D_3$. This process is not influenced by the state of cellular differentiation. Our data also suggest that $1,25(OH)_2D_3$-induced nuclear import is balanced by nuclear export in Caco-2 cells. In addition, our data are consistent with an essential role for nuclear import of VDR in the genomic responses of enterocytes to $1,25(OH)_2D_3$.

EXPERIMENTAL PROCEDURES

Supplies

Unless otherwise noted, all chemicals were obtained from Sigma (St. Louis, MO), cell culture reagent were obtained from Cambrex (Rockland, ME), and cell culture plasticware from Corning-Costar (Cambridge, MA). 1,25 $(OH)_2D_3$ was purchased from Biomol International (Plymouth Meeting, PA). The 1,25 $(OH)_2D_3$ analog, 1α-fluoro-16-ene-20-epi-23-ene-26,27-bishomo-25-hydroxyvitamin D_3 (Ro-26-9228) was kindly provided by Dr. Milan Uskokovic (Roche Bioscience) and its biological actions were previously characterized by Ismail et al. [2004]. $1,25(OH)_2D_3$ and Ro-26-9228 were dissolved in ethanol and kept in light-protected vials at $-80^{\circ}C$. The green fluorescent protein-vitamin D receptor (GFP-VDR) construct used was previously described by Prufer et al. [2000].

Cell Culture

The parental Caco-2 line and the BBe clone of Caco-2 cells were purchased from American Type Cell Culture (HTB-37 and CRL-2102, respectively; ATCC, Rockville, MD). Parental Caco-2 cells were studied between passages 25 and 50, whereas BBe cells were studied between passages 52 and 77. The cells were maintained as described elsewhere [Fleet et al., 2002]. In the experiments reported in this article, we used Caco-2 cells at three different stages of cell differentiation: proliferating, 50% confluent (2-day cells), 2-day post-confluent (6-day cells), and differentiated Caco-2 cells (15-day cells). The parental Caco-2 cell line was used in experiments 1 and 5, while BBe clone was used in experiments 2, 3, and 4 described below. Our previous research demonstrates that both of these Caco-2 lines have all the components necessary for vitamin D regulated transcellular calcium transport [Fleet et al., 2002]. In addition, our initial experiments showed that GFP-VDR distribution and characteristics of VDR trafficking are identical in parental Caco-2 and BBe Caco-2. We chose to use the BBe clone of Caco-2 cells for our imaging analysis reported here because this clone is less morphologically heterogeneous than parental Caco-2 cell line [Peterson and Mooseker, 1992].

The rat osteosarcoma cell line, ROS 17/2.8 (A1G clone), was obtained from Dr. Hector DeLuca (University of Wisconsin, Madison) [Arbour et al., 1998]. ROS 17/2.8 (A1G) cells are stably transfected with a 25-hydroxyvitamin D_3 24-hydroxylase (CYP24)-Luc reporter gene but are otherwise like the parent ROS 17/2.8 line. Cells were maintained in 1:1 mixture of Ham's Nutrient Mixture F12 (Ham's F12) and high-glucose Dulbecco's Modified Eagle's Medium (DMEM) supplemented with 100 U/L of penicillin, 100 μg/L of streptomycin, 1 mM sodium pyruvate, 100 μM non-essential amino acids, 50 μg/L gentamycin, 2 mM L-glutamine, 10 mM N-2-hydroxyethylpiperazine-N-2-ethanesulfonic acid (HEPES), and 10% fetal bovine serum (FBS). ROS 17/2.8 (A1G) cells were passaged by trypsinization every 3–4 days when the cells were 80% confluent. All experiments were performed in subconfluent ROS 17/2.8 (A1G) cells between passages 3 and 28.

Mouse prostate epithelial cells from VDR knockout mice (MPEC VDR KO cells) were obtained from Dr. Scott Cramer (Wake Forest University Medical School) and maintained as described elsewhere [Barclay and Cramer, 2005].

Experimental Design

Experiment 1. Analysis of changes in endogenous VDR protein abundance and distribution. Two experiments were conducted. First, 15-day cultures of parental Caco-2 cells and proliferating ROS 17/2.8 cells were treated with 100 nM $1,25(OH)_2D_3$ for 1 h and whole cell extracts were prepared as described previously [Ismail et al., 2004]. Next, 15-day cultures of Caco-2 cells treated for 2 h with 10 nM $1,25(OH)_2D_3$ or vehicle (0.01% ethanol) afterwards whole cell and nuclear extracts were prepared using the Active Motif Nuclear Extract Kit (Active Motif, Carlsbad, CA). The total protein concentration in the samples was determined using BioRad protein assay (Hercules, CA). The samples containing 20 μg of total protein were analyzed for VDR and general transcription factor II B (TFIIB) protein levels as described previously [Fleet et al., 2002]. The VDR protein level was normalized to TFIIB protein content in each sample to correct for protein loading. Normalized VDR protein levels were expressed relative to vehicle-treated samples. Three independent experiments were performed; each experiment used three replicates per treatment.

Experiment 2. Baseline distribution of GFP-VDR in Caco-2 and ROS 17/2.8 (A1G) cells. Proliferating (2 day) Caco-2 cells, differentiated (15 day) Caco-2 cells, and proliferating ROS 17/2.8 (A1G) cells were transiently transfected with GFP-VDR expression vector as described below. For each cell type, initial confocal images were captured in the focal plane of the cell where the circumference of the nucleus was the greatest. Additionally, we collected sequential optical sections of the cells and reconstructed 3-D images in order to examine the possibility that VDR may accumulate at specific cellular regions, for example, basolateral or brush border membrane of Caco-2 cells. At least 11 3-D reconstructions were prepared for ROS17/2.8 (A1G) and proliferating and differentiating Caco-2 cells.

Experiment 3. The effect of $1,25(OH)_2D_3$ on steady state distribution of GFP-VDR in Caco-2 and ROS 17/2.8 (A1G) cells. Proliferating Caco-2 and ROS17/2.8 (A1G) cells were transiently transfected with GFP-VDR. For each cell, we collected series of two images: a baseline distribution of GFP-VDR and the cellular distribution of GFP-VDR 30 min after treatment with either 100 nM $1,25(OH)_2D_3$ or control solution (0.01% ethanol). For each image in the series we calculated the intensity of fluorescent signal associated within the nuclear and cytoplasmic compartment. Six cells were examined for each cell type and each treatment. Procedures for the analysis of each image are described in detail below in '*Image collection and data analysis*'.

Experiment 4. The effect of $1,25(OH)_2D_3$ on GFP-VDR movement into the nucleus.

Time course of GFP-VDR import in Caco-2 cells following $1,25(OH)_2D_3$ treatment. To study the kinetics of GFP-VDR movement into the nucleus of BBe, we collected a series of nine images of vehicle (0.01% ethanol) or $1,25(OH)_2D_3$ (100 nM) treated cells. After collecting a baseline image, an 8 μm^2 area within nucleus was photobleached using 100% laser power for 10 s and an image showing a bleached nucleus was recorded. Immediately after photobleaching the treatment solution containing either 100 nM $1,25(OH)_2D_3$ or vehicle was added to the well and a series of post-bleach images was recorded at 2.5, 5, 10,

15, 20, 25, and 30 min using the same laser intensity as for the post-photobleaching image. Six cells were examined for each cell type and each treatment. Procedures for the analysis of each image are described in detail below in '*Image collection and data analysis*'.

Early and late fluxes of GFP-VDR into the nucleus. To determine whether the early flux of GFP-VDR after $1,25(OH)_2D_3$ treatment continues throughout the hormone treatment period, we compared the effect of $1,25(OH)_2D_3$ on nuclear import under two different protocols. The first was identical to that described above (photobleaching at $t=0$, treatment with $1,25(OH)_2D_3$, examination of import at $t=5$ min). For the second protocol $1,25(OH)_2D_3$ treatment was initiated at $t=0$ min and photobleaching of the cell nucleus was conducted 30 min afterwards. The post-bleach image was collected after 5 min recovery time. Six cells were examined for each cell type and each treatment. Procedures for the analysis of each image are described in detail below in '*Image collection and data analysis*'.

Control experiments for photobleaching. To evaluate potential confounding influences of the photobleaching protocol used in this experiment we conducted two control experiments. In the first experiment we used a propidium iodide (PI) (Molecular Probes, Inc.) exclusion test to ensure that our photobleaching conditions do not compromise the viability of the cells. In this test, Caco-2 cells were incubated with 2 μg/ml PI for 5 min at 37°C. Following the incubation period, the cells were photobleached as described above. Images were collected over a 30 min period to determine whether the photobleaching technique induced cell death and PI staining of the nuclei. As expected, photobleaching did not increase cell permeability to PI. The second control experiment was conducted to ensure that any increase in fluorescence signal observed during our experiments is not due to de novo synthesis of proteins. To examine this, we completely photobleached the target cell and monitored the changes in fluorescent signal intensity of this cell within next 30 min. As expected no fluorescence signal was observed after 30 min demonstrating that the photobleached fluorochrome is destroyed and that the changes in fluorescent signal intensity we see are not due to de novo protein synthesis of GFP-VDR.

Experiment 5. Ability of VDR ligand to stimulate nuclear import of GFP-VDR correlates with its transcriptional efficacy. The goal of our final experiment was to compare the effects of $1,25(OH)_2D_3$ and its analog, Ro-26-9228 on three functional parameters of VDR action: nuclear import, association of VDR with chromatin, and gene expression in 2-day post-confluent parental Caco-2 cells. In the first part of this experiment, we determined the effect of two VDR ligands on GFP-VDR nuclear import using our established protocol. Briefly, photobleaching of the cell nucleus was followed by immediate addition of treatment solution containing 100 nM $1,25(OH)_2D_3$, 100 nM Ro-26-9228 or vehicle. The post-bleach image was recorded 5 min after photobleaching. For each treatment group at least six image series were quantified as described in '*Image collection and data analysis* Section'. In the second part of this experiment, we examined the impact of $1,25(OH)_2D_3$ treatment on the association of VDR with chromatin. Caco-2 cells (2-day post-confluent) were treated for 1 h with 100 nM $1,25(OH)_2D_3$, Ro-26-9228, or vehicle. Chromatin fractions were isolated and VDR association with chromatin was assessed as described previously [Ismail et al., 2004]. In the final experiment in this section we examined the transcriptional response of the CYP24 gene to 100 nM $1,25(OH)_2D_3$ and 100 nM Ro-26-9228. Two days after reaching confluency Caco-2 cells were treated with 5% FBS containing DMEM with 100 nM $1,25(OH)_2D_3$, 100 nM Ro-26-9228, or vehicle (0.01% ethanol). To better evaluate the effect of two ligands on induction of CYP24 gene expression we used two complementary experimental designs. In the first a 5 min-pulse with treatment solutions was followed by 7 h 55 min incubation with 5% FBS media to allow accumulation of the message ($n=3$ per treatment). In the second design, cells were continually treated with vitamin D compounds for 8 h prior to harvest ($n=3$ per treatment). Cells were harvested into 1 ml of Tri-Reagent and RNA was isolated following the manufacturer's instructions (Molecular Research Center, Cincinnati, OH). The real-time-polymerase chain reaction (PCR) was conducted as described elsewhere [Song et al., 2003b] using the primers: CYP24 forward, CTCATGCTAAATACCCAGGTG, CY P24 reverse, TCGCTGGCAAAACGCGATGGG,GA PDH forward 5′-TCACCATCTTC CAGGAGCG-3′, GAPDH reverse 5′-CTGCTTC ACCACCTTCTTGA-3′ and common for both

primer sets annealing temperature of 54°C. The GAPDH mRNA levels were used as an internal control because expression of this gene does not change in response to $1,25(OH)_2D_3$ treatment. *Transfection of cells with GFP-VDR*. We used two protocols depending on whether we wanted to image proliferating or post-confluent cultures. In proliferating cells, 1 million cells in suspension were transiently transfected immediately following trypsinization using 6 μg of GFP-VDR vector and a 1:2.6:2.6 ratio of DNA/Lipofectamine/Plus Reagent. The cells were then seeded at a density of approximately 30,000 cells per well in an 8-chambered glass coverslip (Nalge Nunc Intl., Rochester, NY). For post-confluent non-proliferating Caco-2 cells an alternate protocol was needed to overcome the low transfection efficiency in non-proliferating cells. For this study, cells were seeded at the density of 21,333 cell per well of an 8-chamber glass coverslip and each well was transfected with 4 μg of GFP-VDR at either 2 or 9 days post-confluence using 1:1:1 ratio of DNA/Lipofectamine/Plus Reagent. With both protocols, cells were used for experiments 2 days after transfection.

Cell culture treatments. In order to avoid the effect of estrogenic agonists present in phenol red (PR) and serum on VDR distribution in living cells [Barsony et al., 1990], the cells transfected with GFP-VDR were routinely switched from their usual medium (2-day Caco-2: DMEM + 20% FBS; post-confluent Caco-2: DMEM + 10% FBS; ROS 17/2.8 (A1G) cells: Ham's F12/DMEM + 10% FBS) to PR-free medium plus 1% insulin–transferrin–selenium (ITS, Invitrogen, Carlsbad, CA) at least 24 h prior imaging session. The treatment solutions containing 100 nM $1,25(OH)_2D_3$, 100 nM Ro-26-9228 or vehicle (ethanol at final concentration of 0.01%) were prepared in this medium and kept at 37°C water bath during imaging sessions.

Image Analysis

Criteria of choosing cells for imaging. Prior to each imaging session we evaluated cell morphology to ensure that cells were viable and healthy. Only cells that had no obvious disruption in their normal morphology were used for imaging. In addition, we avoided using cells with a low fluorescence signal as it would prevent us to use them in our protocols designed to monitoring import of GFP-VDR into the nucleus (where significant signal is lost during initial photobleaching and additional photobleaching occurs during the collection of the subsequent image collection). We also excluded cells of extremely high intensity of the signal since excessive expression of GFP-VDR construct may not reflect physiologic conditions.

Image Collection and Data Analysis

All images in this study were collected using a BioRad MRC 1024 system and the Lasersharp software package (BioRad Laboratories, Richmond, CA). BioRad MRC1024 is equipped with a water-cooled, coherent Innova Enterprise Model 622 Argon Ion UV/VIS laser, a Krypton–Argon Model 5470K laser, a Nikon Diaphot 300 inverted microscope (Nikon Corp., Tokyo, Japan), a Plan APO 60X 1.4 DIC oil objective and a heated stage. All images were collected with the heated stage set at 37°C. To detect GFP-VDR fluorescence, the 488 nm line of a krypton–argon laser was used for excitation of the sample with a bandpass 522/35 emission filter. In PI exclusion test we used the 488 nm krypton–argon laser line with a 605/32 emissions filter.

The creation of 3-D reconstructions from confocal images was accomplished using the MetaMorph software program (Molecular Devices Corporation, Sunnyvale, CA). The quantification of captured images was conducted using Adobe Photoshop (Version 6.0, Adobe System Inc., San Jose, CA).

Measurements of total, nuclear, and cytosolic GFP-VDR content were made for each cell using the histogram function to calculate the total number of pixels and the mean signal intensity per pixel. Intensity of fluorescent signal associated with each cellular compartment was calculated by multiplying the number of pixels by the mean signal intensity per pixel. Fluorescent signal intensity was used to quantitate data from all of our experiments. In experiments 2 and 3 we directly used values of fluorescent signal intensity to determine subcellular distribution of GFP-VDR within the nucleus and cytoplasm. In experiment 3, these values were used to calculate the percentage change in fluorescent signal intensity associated with nucleus of cells from baseline (image 1) due to treatment (image 2). In experiments 4 and 5, we normalized the total fluorescent signal intensity of each cell to a relative value of 5×10^6 and nuclear fluorescent signal intensity after photobleaching was assigned a value equal to 0. The absolute change in nuclear

fluorescent signal intensity over time was calculated for each experimental condition. In addition, we determined the efficiency of photobleaching for each image series. For data quantification we used only those image series for which efficiency of photobleaching was greater than 50%.

Analysis of GFP-VDR Functionality in MPEC VDR KO Cells Using Reporter Gene Assay

MPEC VDR KO cells were transiently cotransfected with 5 μg of rat −298 to +74 bp 24-hydroxylase promoter luciferase gene construct [Kerry et al., 1996], 50 ng of pRL-CMV (Renilla expressing vector for assessing transfection efficiency, Promega, Madison, WI) and 5 μg of a VDR expression vector (GFP-VDR or pCR3-VDR) or pCR3.1-CAT (negative control) using the Lipofectamine Plus procedure (1:4:10 DNA/Lipofectamine/Plus reagent, Invitrogen). Eighteen hours after transfection MPEC VDR KO cells were treated with 100 nM $1,25(OH)_2D_3$ or vehicle for 8 h. The cells were harvested and luciferase activity assay was measured as per the procedures in the Promega Dual Luciferase Assay (Promega).

Statistical Analysis

Data are reported as the means ± the standard error of the mean. The treatment effects in each experiment were compared by one-way ANOVA using the SYSTAT statistical software package (SYSTAT 7.0, Chicago, IL). Pairwise comparisons were conducted when appropriate using Fisher's Protected LSD. Differences between means were considered significant at $P < 0.05$.

RESULTS

Analysis of Changes in Endogenous VDR Protein Abundance in Response to $1,25(OH)_2D_3$

Using standard immunoblotting techniques VDR protein levels were elevated threefold by $1,25(OH)_2D_3$ treatment in ROS cells following 1 h incubation with 100 nM $1,25(OH)_2D_3$ (Fig. 1A). In contrast we did not observe an increase in endogenous VDR protein abundance in parental Caco-2 cells. In addition, Figure 1B shows that ligand does not significantly alter the proportion of endogenous VDR in the nuclear extracts (1.2 ± 0.2 after vitamin D treatment vs. 1.0 ± 0.16 arbitrary units for control, $P = 0.4299$, n = 9) or in the whole cell extracts ($P = 0.9768$, n = 9) from Caco-2 cells, even though we have previously shown that this dose can activate CYP24 and TRPV6 mRNA accumulation in Caco-2 cells [Fleet et al., 2002].

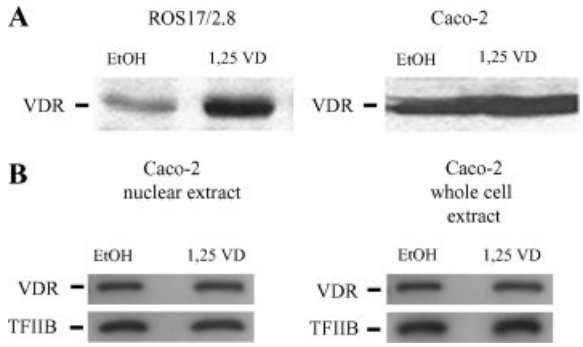

Fig. 1. The effect of $1,25(OH)_2D_3$ on endogenous VDR in Caco-2 and ROS 17/2.8 cells. (**A**) ROS 17/2.8 and parental Caco-2 cells were treated with either 100 nM $1,25(OH)_2D_3$ (1,25 VD) or vehicle (EtOH) for 1 h and VDR protein levels were determined in whole cell extracts by Western blot analysis. (**B**) Caco-2 cells were treated with either 10 nM $1,25(OH)_2D_3$ (1,25 VD) or vehicle (EtOH) for 2 h. Whole cell and nuclear extracts were examined for VDR protein levels by Western blot analysis. The figures are representative blots of individual samples from experiments with n = 3 replicates; experiments were conducted three times.

The Baseline and $1,25(OH)_2D_3$-Induced Effects on the Distribution of GFP-VDR in BBe and ROS17/2.8 (A1G) Cells

Using a transcriptionally functional GFP-VDR construct (i.e., it restored vitamin D-inducible CYP24 promoter activity in VDR null cells, data not shown) we examined basal and $1,25(OH)_2D_3$-induced effects on the subcellular distribution of GFP-VDR in proliferating BBe and ROS17/2.8 (A1G) cells. Figure 2 shows that without hormone, GFP-VDR was evenly distributed within the cytoplasm and nucleus of

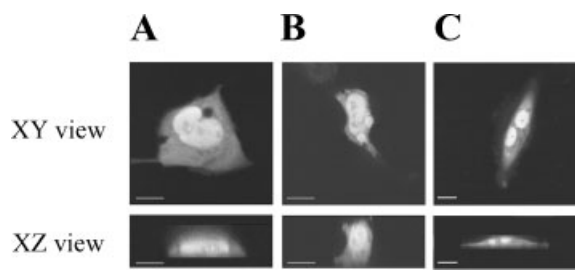

Fig. 2. The distribution of GFP-VDR in proliferating BBe cells (**A**), differentiated BBe cells (**B**), and ROS 17/2.8 (AIG) cells (**C**). Confocal images of GFP-VDR distribution in a single optical section through the center of the cells in two axes: the XY plane and the XZ plane (reconstructed from multiple images in the XY plane).

BBe and ROS 17/2.8 (A1G) cells. Consistent with previous reports (Racz and Barsony, 1999) the nucleoli were devoid of GFP-VDR signal. No GFP-VDR signal was associated with either the apical or basolateroal membranes.

Quantitative analysis revealed significant differences in partitioning of GFP-VDR between cytoplasm and nucleus between BBe and ROS 17/2.8 (A1G) cells. In untreated Caco-2 cells, the GFP-VDR is equally distributed in the nuclear and cytoplasmic compartments (Table I). In contrast, the majority of GFP-VDR resides in the cytoplasm of ROS17/2.8 (A1G) cells and only a small portion is associated with the nucleus ($28.48 \pm 1.71\%$). Proliferating and differentiated Caco-2 cells had similar amount of nuclear GFP-VDR indicating that the process of differentiation to the absorptive phenotype did not affect the subcellular distribution of GFP-VDR.

In ROS 17/2.8 (A1G) cells treatment of cells with 100 nM $1,25(OH)_2D_3$ for 30 min increased the percentage of nuclear GFP-VDR from 28 to 37%. Treatment with 100 nM $1,25(OH)_2D_3$ did not increase nuclear accumulation nor did it reduce the cytoplasmic signal of GFP-VDR in BBe cells (Fig. 3).

The Effect of $1,25(OH)_2D_3$ on Nuclear Import of GFP-VDR

By photobleaching the GFP signal in the nucleus we were able to minimize the impact of nuclear export in our analysis and directly visualize nuclear import of GFP-VDR in BBe cells. As shown in Figure 4, ligand-independent nuclear accumulation of GFP-VDR occurred in both proliferating and differentiated BBe cells. Accumulation of GFP-VDR was significantly accelerated by $1,25(OH)_2D_3$ treatment; the increase was significant within 2.5 min of treatment and this difference was maintained throughout the 30 min study period. At 5 min, nuclear content of the vehicle-treated cells had increased by 13% while the $1,25(OH)_2D_3$ treatment increased nuclear GFP-VDR levels by 30%. $1,25(OH)_2D_3$-mediated accumulation of GFP-VDR in the nucleus became saturated after 25–30 min, a point where the distribution of GFP-VDR between the nucleus and cytoplasm had reached pre-photobleaching levels. This suggests either that GFP-VDR import slowed over time or that equilibrium was reached between nuclear import and export during the 30 min study period.

TABLE I. The Distribution of GFP-VDR in BBe and ROS 17/2.8 (A1G) Cells

Cell type	% Nuclear	% Cytosolic
ROS 17/2.8	28.48 ± 1.71	71.51 ± 1.71
BBe (2, days-culture)	53.93 ± 2.22	46.06 ± 2.22
BBe (15, days-culture)	51.43 ± 2.52	48.57 ± 2.52

Confocal images from transiently transfected cells were quantified and analyzed as described in the *Materials and Methods* Section. The data represent mean ± SEM of the fluorescent signal intensity associated with nucleus and cytoplasm ($n = 12$ or more per cell type).

Early and Late Fluxes of GFP-VDR Into Nucleus

To distinguish between the alternative hypotheses explaining the saturation of nuclear GFP-VDR accumulation following treatment with $1,25(OH)_2D_3$ (i.e., slowing over time vs. balancing of import and export) we examined movement of GFP-VDR into the nucleus of BBe cells during the early and late phase of the response to hormone. Consistent with our initial observation, accumulation of GFP-VDR in $1,25(OH)_2D_3$-stimulated cells was twice as high as control cells within 5 min of treatment (Fig. 5A). Similarly, we found that GFP-VDR accumulation in $1,25(OH)_2D_3$-treated cells was 158.7% higher than in vehicle-treated cells when flux was examined 30 min after treatment (Fig. 5B). These data demonstrate that $1,25(OH)_2D_3$-induced nuclear import of GFP-VDR in BBe cells is continuous throughout the 30 min period we examined.

Ability of VDR Ligand to Stimulate Nuclear Import of GFP-VDR Correlates With its Transcriptional Efficacy

We have previously shown that the analog Ro-26-9228 had reduced transcriptional potency in Caco-2 cells as compared to the effect of the analog in the hFOB osteoblast cell line [Ismail et al., 2004]. This was partially explained by reduced ability of analog-bound VDR to interact with essential protein partners, for example, RXR and glucocorticoid receptor interacting protein 1 (GRIP1). Others have observed that ligand-dependent nuclear import of VDR is dependent upon interactions between VDR and importin α [Yasmin et al., 2005]. With this in mind, we compared the ability of $1,25(OH)_2D_3$ and Ro-26-9228 to induce nuclear GFP-VDR accumulation and subsequent downstream events: association of VDR with

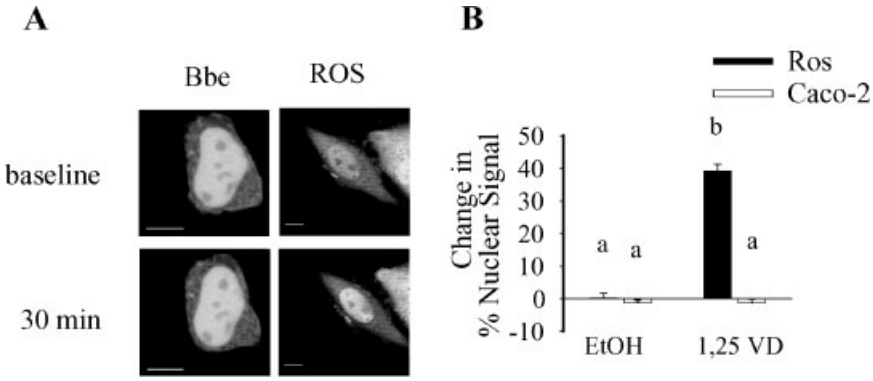

Fig. 3. Calcitriol causes significant changes in distribution of GFP-VDR in ROS 17/2.8 but not in BBe cells. The images of proliferating BBe cells or ROS17/2.8 (A1G) cells were taken before (baseline) and 30 min after incubation with 100 nM $1,25(OH)_2D_3$. (**A**) Representative confocal images. (**B**) Image analysis of n = 6 cells per cell type and treatment. The change in % signal intensity was calculated as described in *Materials and Methods* Section. Data represent mean ± SE. Values with different superscripts are significantly different from one another ($P < 0.05$, n = 6 cells per treatment).

chromatin, and CYP24 mRNA accumulation in post-proliferating parental Caco-2 cells.

As Figure 6A shows, both $1,25(OH)_2D_3$ and Ro-26-9228 increased GFP-VDR nuclear import within 5 min of treatment. However, while the natural ligand increased nuclear GFP-VDR by 99% compared to vehicle, the effect of the analog was significantly blunted (40% increase). The ligand-induced association of endogenous VDR with chromatin was also 60% lower in

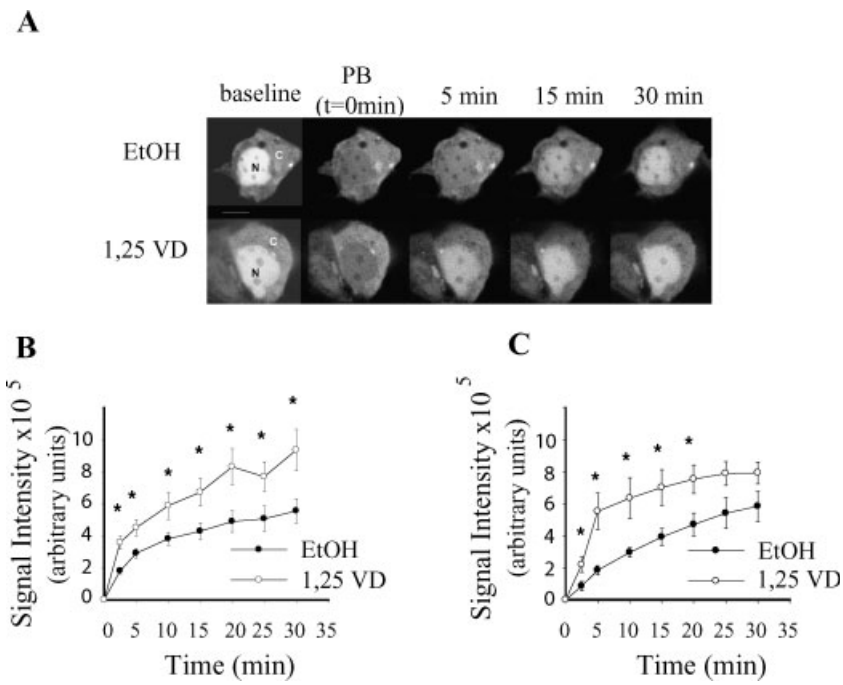

Fig. 4. Calcitriol stimulates rapid translocation of GFP-VDR to the nucleus of BBe cells. **A**: Representative time series for a single differentiated BBe cell response to 100 nM $1,25(OH)_2D_3$ (1,25 VD) or vehicle (EtOH), (**B**) summary of the response to $1,25(OH)_2D_3$ in proliferating BBe cells, (**C**) summary of the response to $1,25(OH)_2D_3$ in differentiated BBe cells. Nuclear photobleaching of GFP-VDR transfected cells was conducted at t = 0, a baseline image was collected and immediately afterwards cells were treated with either 100 nM $1,25(OH)_2D_3$ (1,25 VD) or vehicle (EtOH). Images of cells were taken at 2.5, 5, and every 5 min until 30 min. Points represent the mean ± SEM of n = 6 cells per treatment. * Values for a time point are significantly different between vehicle and vitamin D treated cells, $P < 0.05$.

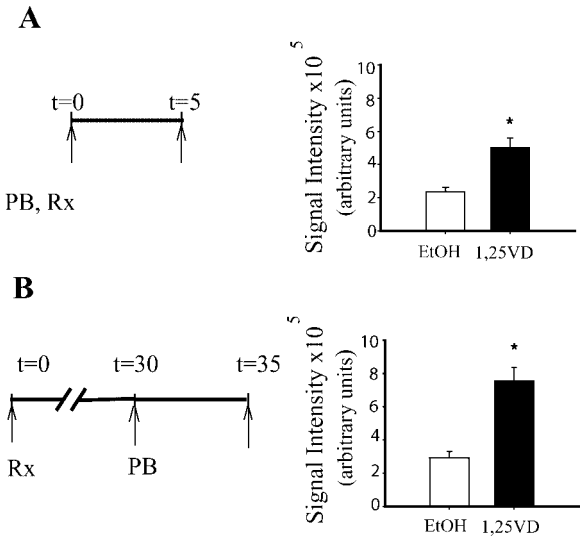

Fig. 5. Nuclear import of GFP-VDR occurs throughout a 30 min period of treatment with $1,25(OH)_2D_3$ in BBe cells. Nuclear accumulation of GFP-VDR was examined at an early (5 min, **A**) and later (30 min, **B**) period after treatment of 6-day cultures of BBe cells with 100 nM $1,25(OH)_2D_3$ (1,25 VD) or vehicle (EtOH). (**A**) Nuclear import at 5 min after treatment. The graphic on the left represents the photobleaching (PB), treatment (Rx) and image collection times (arrows). (**B**) Nuclear import at 30 min after addition of $1,25(OH)_2D_3$ or vehicle. In the late assessment period protocol, cells were treated with 100 nM $1,25(OH)_2D_3$ or vehicle at t = 0. Thirty minutes later nuclei were photobleached and an image was collected. A second image was collected 5 min later. The confocal images were analyzed as described in *Materials and Methods* Section. Data represent mean ± SEM (n = 6 per treatment). Values with an asterisk are significantly different from one another ($P < 0.05$).

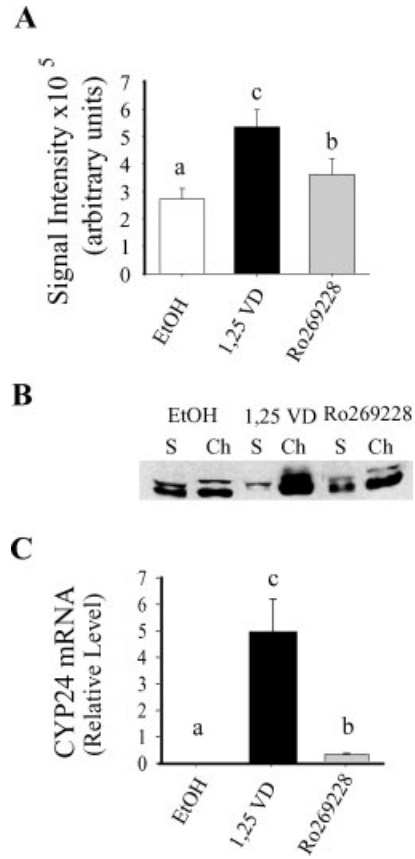

Fig. 6. The ability of VDR ligands to stimulate VDR nuclear import in parental Caco-2 cells is associated with their transcriptional efficacy. (**A**) The effect of 5 min treatment with 100 nM $1,25(OH)_2D_3$, 100 nM Ro269228, or vehicle (EtOH) on GFP-VDR nuclear import. Bars represent mean ± SEM (n = 6). (**B**) The effect of 1 h treatment with 100 nM $1,25(OH)_2D_3$, Ro269228, or vehicle (EtOH) on the association of endogenous VDR with chromatin. The figure is representative data from a single sample per treatment group. S, soluble; Ch, chromatin. (**C**) The effect of a pulse treatment (5 min treatment, 7 h 55 min vehicle) with either 100 nM $1,25(OH)_2D_3$, Ro269228, or vehicle (EtOH) on CYP24 mRNA levels as determined by RT-PCR analysis. CYP24 mRNA levels are normalized to GAPDH mRNA levels within the samples. Bars represent mean ± SEM (n = 3 per treatment); the experiment was repeated three times with similar results. Values with different superscripts are significantly different from one another ($P < 0.05$).

analog-treated compared to $1,25(OH)_2D_3$-treated cells: threefold increase for Ro-26-9228 versus eightfold increase for $1,25(OH)_2D_3$ (Fig. 6B). Finally, CYP24 mRNA accumulation was significantly lower for the analog-treated cells in both the pulse and continuous treatment protocols. For the pulse treatment protocol, the accumulation of CYP24 mRNA following analog treatment was only 6% of that observed with natural ligand (Fig. 6C). Interestingly, continuous treatment minimized the discrepancy in CYP24 mRNA accumulation between the natural ligand and the analog (analog response = 58% of the natural ligand, data not shown) demonstrating partial compensation for the blunted analog response. Altogether, these data show that the analog Ro-26-9228 had reduced ability to stimulate GFP-VDR nuclear import and that this was reflected in a suppression of downstream events, for example, DNA binding and gene expression.

DISCUSSION

In this study we examined the distribution of VDR in the enterocyte-like cell line Caco-2 and we found several interesting features of VDR distribution and mobility unique to this critical vitamin D target cell.

First, our quantitative analysis showed that approximately equal levels of GFP-VDR reside in the cytoplasm and nucleus of Caco-2 cells in the absence of $1,25(OH)_2D_3$. In contrast, we

found that the baseline GFP-VDR distribution in ROS17/2.8 (A1G) cells was predominantly cytoplasmic (>70%), a finding that confirms what others have reported for VDR distribution in ROS 17/2.8 cells [Racz and Barsony, 1999], COS-1 (Sunn et al., 2001), and COS-7 [Racz and Barsony, 1999] kidney cells, and microwave-fixed fibroblasts [Barsony et al., 1990]. Next, we observed that the signal produced by our GFP-VDR construct was diffusely distributed within the nucleus. This is similar to what Sunn et al. [2001] previously reported for an enhanced GFP-labeled version of the traditional VDR-A isoform in COS-1 cells. Thus, although others have reported that the traditional VDR can be found in caveolin-rich membrane domains in chick intestinal cells and in ROS 17/2.8 cells [Huhtakangas et al., 2004], we did not observe any accumulation of GFP-VDR near either the apical or basolateral membrane in our 3-D reconstructions. Our observation is consistent with what Barsony et al. [1997] reported using a BODIPY-labeled $1,25(OH)_2D_3$ in human fibroblasts. This does not support a role for a membrane-associated VDR as the mediator responsible for the activation of various kinases and signal transduction pathways by $1,25(OH)_2D_3$ that have been observed in a variety of cell types [Fleet, 2004], including Caco-2 cells [Wali et al., 1992; Tien et al., 1993; Bettoun et al., 2003]. However, our inability to see membrane-associated GFP-VDR could reflect several factors including low sensitivity of the method to detect the 1–3% of VDR that is proposed to be associated with the membrane or an inability of the GFP-VDR to associate with the membrane.

Another interesting finding from our experiments is that neither endogenous VDR nor GFP-VDR accumulate in the cell or in the nucleus following $1,25(OH)_2D_3$ treatment. This is in contrast to previous reports that consistently show a significant accumulation of VDR resulting from $1,25(OH)_2D_3$-induced protein stabilization in other cell types [Mahonen and Maenpaa, 1994; Masuyama and MacDonald, 1998; Jaaskelainen et al., 2000]. Our data in Caco-2 cells are consistent with a report by Wiese et al. [1992] who found that $1,25(OH)_2D_3$ treatment had modest (twofold), delayed (>4 h), and transient (normal VDR levels by 24 h) effect on VDR protein levels in the rat intestinal crypt-like cell line IEC-6. Neither this study, nor our data explain why $1,25(OH)_2D_3$ stabilization of VDR in the enterocyte is less dramatic than in other cell types. However, even though we did not observe accumulation of total or nuclear VDR levels in Caco-2 cells after $1,25(OH)_2D_3$ treatment, we did find that the distribution of the receptor within the nucleus shifts towards a greater association with the chromatin fraction following 1 h of treatment. Thus, the lack of nuclear VDR accumulation masks the activation of VDR as a transcription factor.

In contrast, using photobleaching to reduce GFP-VDR signal in the nucleus allowed us to document $1,25(OH)_2D_3$-dependent nuclear import of GFP-VDR in Caco-2 cells. This increase was substantial and continuous in the presence of hormone. The difference between ligand-dependent and ligand-independent import accounted for a 20% increase in nuclear level of GFP-VDR per 5 min period; this was true whether we examined vitamin D-induced GFP-VDR movement immediately after or 30 min after hormone treatment. The mechanism mediating the nuclear import of GFP-VDR in Caco-2 cells is unclear. Ligand-independent import has been shown to be dependent upon importin 4 (Miyauchi et al., 2005) and also requires nuclear localization signals within its heterodimeric partner RXR [Prufer and Barsony, 2002]. In contrast, ligand-induced VDR movement occurs independent of the RXR nuclear localization signal [Prufer and Barsony, 2002] and a recent report by Yasmin et al. [2005] suggests that $1,25(OH)_2D_3$-induced VDR-RXR nuclear import is due to recruitment of importin α to the VDR.

Our data from photobleaching experiments demonstrates that vitamin D-induced nuclear import should be sufficient to cause nuclear accumulation of GFP-VDR; the import rate we documented was sufficient to transfer at least 36% of the cytoplasmic signal into the nucleus in the 30 min period we studied. While we did not directly evaluate nuclear GFP-VDR export, we believe that the lack of GFP-VDR accumulation in the presence of ligand in non-photobleached cells, even in the face of significant nuclear import, is consistent with the hypothesis that VDR import and export are balanced in enterocytes. Cell-specific differences in nuclear accumulation of VDR following vitamin D treatment may therefore be due to differences in the efficiency of vitamin D-induced GFP-VDR export. Unfortunately the mechanism mediating ligand-induced nuclear export of steroid

hormone receptor superfamily members, especially VDR, is not clear [Pemberton and Paschal, 2006]. For example, while chromosomal region maintenance 1 protein (CRM-1) receptor-mediated export is important for nuclear export of the unliganded VDR, ligand-enhanced export of VDR is CRM-1 independent [Prufer and Barsony, 2002]. Alternately, $1,25(OH)_2D_3$-induced nuclear export may be mediated by binding to calreticulin, a protein previously identified as important for the export of multiple members in nuclear hormone receptor superfamily including VDR [Black et al., 2001]. However, a recent study by Walther et al. [2003] suggests that the previously identified role for calreticulin in the nuclear export of the glucocorticoid receptor is an artifact of the heterokaryon method used to identify calreticulin as a critical nuclear export protein. Other mechanisms have also been proposed to mediate nuclear export of steroid hormone receptor family members. For example, Saporita et al. [2003] identified amino acid sequences in helixes 5–8 of the ligand binding domain that were involved in the nuclear export of the androgen receptor, the mineralcorticoid receptor, and estrogen receptor α. Unfortunately, the residues proposed to be critical for nuclear export in those receptors are not well conserved in the VDR (data not shown). Future studies will be necessary to identify the critical proteins mediating export of VDR and other nuclear receptor members.

In our final study we examined the relationship between $1,25(OH)_2D_3$ or Ro-26-9228-induced VDR import and downstream events following in Caco-2 cells, that is, association of VDR with chromatin, mRNA accumulation. Previous studies showed that Ro-26-9228 works as a tissue selective $1,25(OH)_2D_3$ analog characterized by a tenfold lower ability to induce gene transcription in intestinal epithelial cells compared to osteoblasts [Ismail et al., 2004]. This was due in part to reduced ability of analog-bound VDR to form essential protein–protein interactions with its heterodimeric partner RXR as well as the coactivator GRIP1. Here, we add to this story by showing that the earliest step of the vitamin D-signaling process, measured by nuclear import of GFP-VDR, was less efficient in the presence of analog compared to the natural ligand. Reduced nuclear import was associated with a reduction in the next step in the process of transcription: association of VDR with chromatin. This was subsequently reflected as reduced ligand-induced CYP24 mRNA accumulation. While the role of reduced analog-induced binding of the coactivator GRIP1 to VDR is certainly contributing to the reduced transcription of the CYP24 gene, our data are consistent with the observations of Racz and Barsony [1999], who found that VDR nuclear translocation is a critical component of the receptor activation process and vitamin D-mediated gene transcription. In addition, this observation is consistent with the hypothesis that conformational changes in VDR induced by vitamin D analogs not only affect its interactions with RXR and coactivators [Ismail et al., 2004] but also with proteins critical for nuclear VDR import, that is, importins.

ACKNOWLEDGMENTS

The authors would like to thank Dr. J. Paul Robinson and the staff of the Purdue Cytometry Laboratory for their assistance with the confocal microscopy. The Purdue Cytometry lab is supported in part by the Purdue Cancer Center (CA 23168). This work was funded by NIH grants DK54111 (to J.C.F.) and DK50583 (to S.P.).

REFERENCES

Arbour NC, Ross TK, Zierold C, Prahl JM, DeLuca HF. 1998. A highly sensitive method for large-scale measurements of 1,25-dihydroxyvitamin D. Anal Biochem 255:148–154.

Barclay WW, Cramer SD. 2005. Culture of mouse prostatic epithelial cells from genetically engineered mice. Prostate 63:291–298.

Barsony J, Pike JW, DeLuca HF, Marx SJ. 1990. Immunocytology with microwave-fixed fibroblasts shows 1 alpha,25-dihydroxyvitamin D3-dependent rapid and estrogen-dependent slow reorganization of vitamin D receptors. J Cell Biol 111:2385–2395.

Barsony J, Renyi I, McKoy W. 1997. Subcellular distribution of normal and mutant vitamin D receptors in living cells. J Biol Chem 272:5774–5782.

Bettoun DJ, Burris TP, Houck KA, Buck DW, Stayrook KR, Khalifa B, Lu J, Chin WW, Nagpal S. 2003. Retinoid X receptor is a non-silent major contributor to vitamin d receptor-mediated transcriptional activation. Mol Endocrinol 17:2320–2328.

Black BE, Holaska JM, Rastinejad F, Paschal BM. 2001. DNA binding domains in diverse nuclear receptor function as nuclear export signals. Curr Biol 11:1749–1758.

Bronner F. 2003. Mechanisms of intestinal calcium absorption. J Cell Biochem 88:387–393.

Fleet JC. 2004. Rapid, membrane-initiated actions of 1,25 dihydroxyvitamin d: What are they and what do they mean? J Nutr 134:3215–3218.

Fleet JC. 2006. Molecular regulation of calcium metabolism. In: Weaver CM, Heaney RP, editors. Calcium in human health. Totowa, NJ: Humana Press, pp 163–190.

Fleet JC, Eksir F, Hance KW, Wood RJ. 2002. Vitamin D-inducible calcium transport and gene expression in three Caco-2 cell lines. Am J Physiol-Gastrointest Liver Physiol 283:G618–G625.

Giuliano AR, Wood RJ. 1991. Vitamin D-regulated calcium transport in Caco-2 cells: Unique in vitro model. Am J Physiol 260:G207–G212.

Haussler MR, Whitfield GK, Haussler CA, Hsieh JC, Thompson PD, Selznick SH, Dominguez CE, Jurutka PW. 1998. The nuclear vitamin D receptor: Biological and molecular regulatory properties revealed. J Bone Miner Res 13:325–349.

Hoenderop JG, Nilius B, Bindels RJ. 2005. Calcium absorption across epithelia. Physiol Rev 85:373–422.

Huhtakangas JA, Olivera CJ, Bishop JE, Zanello LP, Norman AW. 2004. The vitamin D receptor is present in caveolae-enriched plasma membranes and binds 1{alpha},25(OH)2-vitamin D3 in vivo and in vitro. Mol Endocrinol 18:2660–2671.

Ismail A, Nguyen CV, Ahene A, Fleet JC, Uskokovic MR, Peleg S. 2004. Effect of cellular environment on the selective activation of the vitamin D receptor by 1{alpha},25-dihydroxyvitamin D3 and its Analog 1{alpha}-fluoro-16-ene-20-epi-23-ene-26,27-bishomo-25-hydroxyvitamin D3 (Ro-26-9228). Mol Endocrinol 18: 874–887.

Jaaskelainen T, Ryhanen S, Mahonen A, DeLuca H, Maenpaa P. 2000. Mechanism of action of superactive vitamin D analogs through regulated receptor degradation. J Cell Biochem 76:548–558.

Kerry DM, Dwivedi PP, Hahn CN, Morris HA, Omdahl JL, May BK. 1996. Transcriptional synergism between vitamin D-responsive elements in the rat 25-hydroxyvitamin D3 24-hydroxylase (CYP24) promoter. J Biol Chem 271:29715–29721.

Mahonen A, Maenpaa PH. 1994. Steroid hormone modulation of vitamin D receptor levels in human MG-63 osteosarcoma cells. Biochem Biophys Res Comm 205: 1179–1186.

Masuyama H, MacDonald PN. 1998. Proteasome-mediated degradation of the vitamin D receptor (VDR) and a putative role for SUG1 interaction with the AF-2 domain of VDR. J Cell Biochem 71:429–440.

Michigami T, Suga A, Yamazaki M, Shimizu C, Cai G, Okada S, Ozono K. 1999. Identification of amino acid sequence in the hinge region of human vitamin D receptor that transfer a cytosolic protein to the nucleus. J Biol Chem 274:33531–33538.

Miyauchi Y, Michigami T, Sakaguchi N, Sekimoto T, Yoneda Y, Pike JW, Yamagata M, Ozono K. 2005. Importin 4 is responsible for ligand-independent nuclear translocation of vitamin D receptor. J Biol Chem 280: 40901–40908.

Pemberton LF, Paschal BM. 2006. Scientists share nuclear secrets at jekyll island. Traffic 7:751–760.

Peterson MD, Mooseker MS. 1992. Characterization of the enterocyte-like brush border cytoskeleton of the C2BBe clones of the human intestinal cell line, Caco-2. J Cell Sci 102:581–600.

Prufer K, Barsony J. 2002. Retinoid X receptor dominates the nuclear import and export of the unliganded vitamin D receptor. Mol Endocrinol 16:1738–1751.

Prufer K, Racz A, Lin GC, Barsony J. 2000. Dimerization with retinoid X receptors promotes nuclear localization and subnuclear targeting of vitamin D receptors. J Biol Chem 275:41114–41123.

Racz A, Barsony J. 1999. Hormone-dependent translocation of vitamin D receptors is linked to transactivation. J Biol Chem 274:19352–19360.

Saporita AJ, Zhang Q, Navai N, Dincer Z, Hahn J, Cai X, Wang Z. 2003. Identification and characterization of a ligand-regulated nuclear export signal in androgen receptor. J Biol Chem 278:41998–42005.

Song Y, Kato S, Fleet JC. 2003a. Vitamin D receptor (VDR) knockout mice reveal VDR-independent regulation of intestinal calcium absorption and ECaC2 and calbindin D9k mRNA. J Nutr 133:374–380.

Song Y, Peng X, Porta A, Takanaga H, Peng JB, Hediger MA, Fleet JC, Christakos S. 2003b. Calcium transporter 1 and epithelial calcium channel messenger ribonucleic acid are differentially regulated by 1,25 dihydroxyvitamin D3 in the intestine and kidney of mice. Endocrinology 144:3885–3894.

Sunn KL, Cock TA, Crofts LA, Eisman JA, Gardiner EM. 2001. Novel N-terminal variant of human VDR. Mol Endocrinol 15:1599–1609.

Tien XY, Brasitus TA, Qasawa BM, Norman AW, Sitrin MD. 1993. Effect of 1,25 (OH)2 D3 and its analogues on membrane phosphoinositide turnover and [Ca21]i in Caco-2 cells. Am J Physiol 265:G143–G148.

Van Cromphaut SJ, Dewerchin M, Hoenderop JG, Stockmans I, Van Herck E, Kato S, Bindels RJ, Collen D, Carmeliet P, Bouillon R, Carmeliet G. 2001. Duodenal calcium absorption in vitamin D receptor-knockout mice: Functional and molecular aspects. Proc Natl Acad Sci USA 98:13324–13329.

Wali RK, Baum CL, Bolt MJ, Brasitus TA, Sitrin MD. 1992. 1,25-dihydroxyvitamin D3 inhibits Na(+)-H+ exchange by stimulating membrane phosphoinositide turnover and increasing cytosolic calcium in CaCo-2 cells. Endocrinology 131:1125–1133.

Walther RF, Lamprecht C, Ridsdale A, Groulx I, Lee S, Lefebvre YA, Hache RJ. 2003. Nuclear export of the glucocorticoid receptor is accelerated by cell fusion-dependent release of calreticulin. J Biol Chem 278: 37858–37864.

Wiese RJ, Uhland-Smith A, Ross TK, Prahl JM, DeLuca HF. 1992. Up-regulation of the vitamin D receptor in response to 1,25-dihydroxyvitamin D3 results from ligand-induced stabilization. J Biol Chem 267:20082–20086.

Yasmin R, Williams RM, Xu M, Noy N. 2005. Nuclear import of the retinoid X receptor, the vitamin D receptor, and their mutual heterodimer. J Biol Chem 280:40152–40160.